Microstructure and corrosion behaviour of plain carbon steel–B_4C composite produced by GTAW method in 3·5 wt-%NaCl solution

S. H. Ettefagh Far*[1] and A. Davoodi[2]

In this work, the corrosion behaviour of metal matrix composite plain carbon steel–B_4C was studied in 3·5 wt-%NaCl solution. The composite was locally produced as weld band on plain carbon steel by means of gas tungsten arc welding process and using nickel as wetting agent. Samples from weld band, heat affected zone and base regions were extracted precisely, and electrochemical techniques including open circuit potential, linear polarisation resistance, electrochemical impedance spectroscopy, potentiodynamic polarisation in combination with SEM-EDX surface analysis and microhardness were used for characterisation. The results showed that hardness value of made composite increased significantly to 642 HV10. However, the corrosion resistance of composite region during 7 days (168 h) of exposure to 3·5 wt-%NaCl solution was slightly reduced. This was attributed to the fact that B_4C particles play as cathode site for oxygen reduction; therefore, they increase the corrosion rate slightly.

Keywords: Metal matrix composites, Corrosion, Electrochemical impedance spectroscopy, Potentiodynamic polarisation, SEM

Introduction

In the recent years, efforts for finding new materials and reducing economic costs for producing pure components have gained commercial and technological importance.[1] Metal matrix composite (MMC) constitute a new class of materials that are superior to metals and alloys. Adding hard ceramic particles to the metal matrix increases resistance to abrasion and hardness and generates suitable lubrication in MMCs.[2] The examples of common strengthening particles among abrasion resistant substances that can be used in MMCs are B_4C, SiC and Al_2O_3. B_4C is a material with applications in different fields and is selected due to low density (2·51 g cm^{-3}) compared with SiC (3·21 g cm^{-3}), diamond (3·51 g cm^{-3}) and Al_2O_3 (3·92 g cm^{-3}).[1] B_4C is known for its high hardness and resistance to abrasion and leads to increase in resistance to fatigue in the coated zone by its surface lapping. It has also some properties such as elastic module, high melting point and low density.[1,3–5] It is necessary to note that B_4C has been considered due to its high effective cross-section, stability in corrosive solutions[3,6] and electric conduction (2×10^7 s m^{-1}) of its microparticles.[7] Desirable chemical and thermal stability of B_4C is because of its covalent bond.[8] Being used in manufacturing sandblast nozzles[8] and cutting tools and in nuclear industries due to its neutron absorption is among its applications.[9] Plain carbon steel has abundant applications in the industry because of its high strength, suitable welding capability, flexibility, easy availability, excellent physical properties and low price,[10] but its use has been constrained under such conditions due to the resistance to abrasion and low surface hardness. Therefore, surface properties of plain carbon steel can be transformed by making a composite on that. It is not cost effective in the industry to coat the surface by composite and make the parts that are entirely of composites. To obtain their desirable properties, many researchers have directed their studies for manufacturing B_4C composite by nickel, phosphorous and other factors toward metals such as magnesium and aluminium using methods such as electroless and studying its corrosive behaviour in desirable corrosive environments.[11] Nevertheless, this research attempted to locally make plain carbon steel composite with B_4C under local wetting of nickel using gas tungsten arc welding (GTAW) on plain carbon steel and to study its corrosive behaviour in different positions. This method can be used in desired areas on plain carbon steel to locally increase hardness and resistance to abrasion and reduce costs of its manufacturing. The structures containing MMCs are corroded when being exposed to marine atmospheres and marine water drops along with wind.[12] Sea water, by virtue of its chloride content, is an efficient electrolyte.[13] Therefore, because B_4C composite is locally generated on the plain carbon steel surface, its corrosive behaviour becomes important when being exposed to corrosive conditions such as the environments containing chloride ion.

[1]Department of Materials Science and Engineering, Khorasan Razavi, Science and Research Branch, Islamic Azad University, Neyshabur, Iran
[2]Department of Materials Science and Engineering, Faculty of Engineering, Hakim Sabzevari University, Sabzevar 391, Iran

*Corresponding author, email hosseinett@gmail.com

Published by Maney on behalf of the Institute
Received 9 June 2013; accepted 5 August 2013
DOI 10.1179/1743278213Y.0000000110

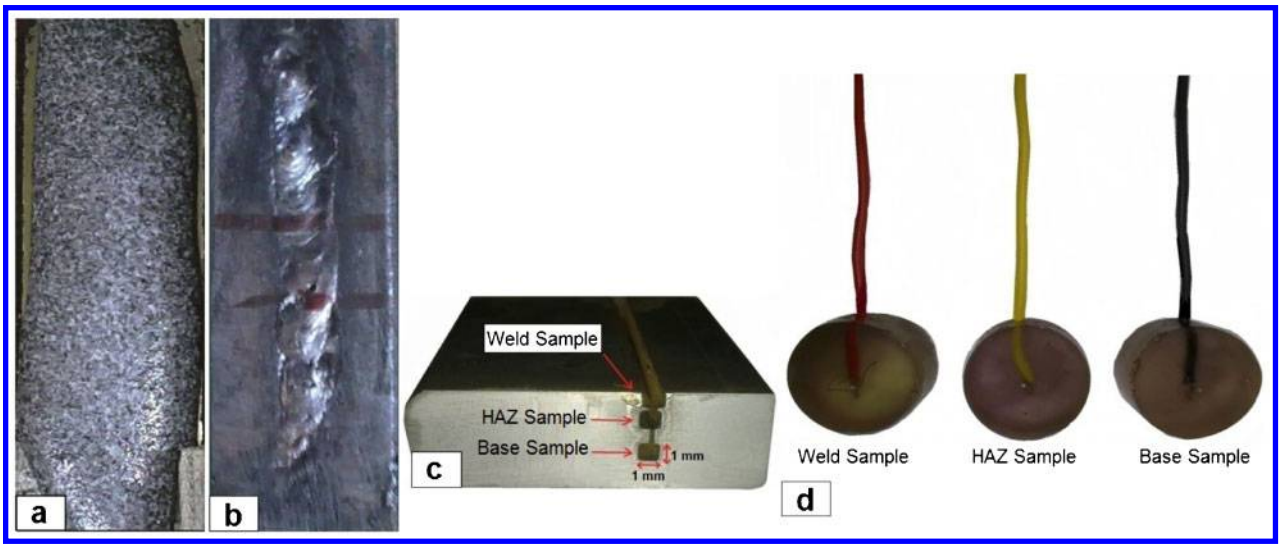

1 Image of *a* powders B_4C and nickel mixed with glue polyvinyl acetate, *b* produced weld band as plain carbon steel/B_4C composite by GTAW method, *c* sample extraction from three regions base, weld and heat affected zone (HAZ) and *d* corrosion test samples

Experimental

Material and methods

Plain carbon steel is used for generating B_4C composite under wetting of nickel using GTAW as the base metal; therefore, it is necessary to determine chemical composition of the base metal. The data of this analysis are given in Table 1.

A sample of plain carbon steel with dimensions of $10 \times 30 \times 100$ mm was cut, and its surface was polished with a polishing machine to remove grease and be deoxidised. Then, it was washed by nitric acid, alcohol and distilled water to prepare the surface for creating the stable arc. An optimised parameter to obtain a desirable composite on surface was used (attaining the optimisation result will be published elsewhere). Polyvinyl acetate glue was saturated with 60 vol.-%B_4C powder with mesh of 125 and 40 vol.-% nickel powder with mesh of 100 and was dispersed on the base metal with the width of 10 mm. Then, the prepared sample was placed inside the electric furnace at 140°C for half an hour in order for the glue mixture on its surface to be dried. Afterwards, the sample was exposed to surface modification operations using the GTAW device in forehand method. It is worth mentioning that no filler was used in welding, but the melt created by arc produced by tungsten electrode in welding on the base metal was used to produce composite in surface modification operations. After welding and making the composite on base metal, the welded sample was transected and cold mounted. The composition of the cold mount was 95% polyester resin + 4% benzoyl acid + 1·1% cobalt. Then, the sample was polished using an 80 to 300 polishing pad and was etched by the etchant solution (composed of 18% nitric acid + 2% hydrofluoric acid + 80% ethanol) for 15 s to conduct microstructural studies. Stages of manufacturing and preparing the composite sample are shown in Fig. 1*a* and *b* respectively.

Table 1 Chemical composition of base metal

Element	Fe	C	Mg	P	Si	S
Composition/wt-%	98·579	0·0667	0·493	0·23	0·01	0·025

In order to study microstructure of the composite and its composition, devices such as SEM test device and VEGA-LMU model, made by Tescan Company in Czech, were used. Micro Cupa Hardness Tester made in Iran was used to measure hardness in terms of HV with the applied force of 10 kgf with Diamond Pyramid Plunger from the base metal to the end of composite welding sample, in which the distance between test points was 1·5 mm.

Electrochemical measurements

The samples were cut from three zones of base sample, weld sample and HAZ sample with dimensions of $1 \times 1 \times 10$ mm using a wire cut device. Images of base sample, weld sample and HAZ sample zones, corrosion test sample which was cut using a wire cut device, are given in (Fig. 1*c*). The area of the sample relating to corrosive environment was 1×1 mm. To keep this area constant, the samples were coated by resin or polymeric materials such as Teflon or polyester with the defined area. The samples prepared from zones of steel base sample, weld sample and HAZ sample were connected to a copper wire with equal resistance and same material for each sample and then were cold mounted. The image of prepared corrosion test samples is shown in (Fig. 1*d*). Ivium corrosion test device, Compact Stat model, made in The Netherlands, was used to perform electrochemical tests. Temperature of the electrolyte solution was 25°C, and a heater with ambient temperature was used to keep the temperature constant during the test stages. The electrolyte solution was 3·5 wt-%NaCl; this solution was used in corrosion cell for electrochemical tests. The pH of the solution was 5·9, and the solution contained air. For each sample, a corrosion cell was prepared, into which the electrolyte solution was poured. The classic corrosion cell, which included a reference electrode as saturated calomel electrode, a working electrode (corrosion test sample) and a graphite counter electrode, was prepared.

Base, weld and HAZ samples, which were mounted for corrosion test, were polished by the 600–1000

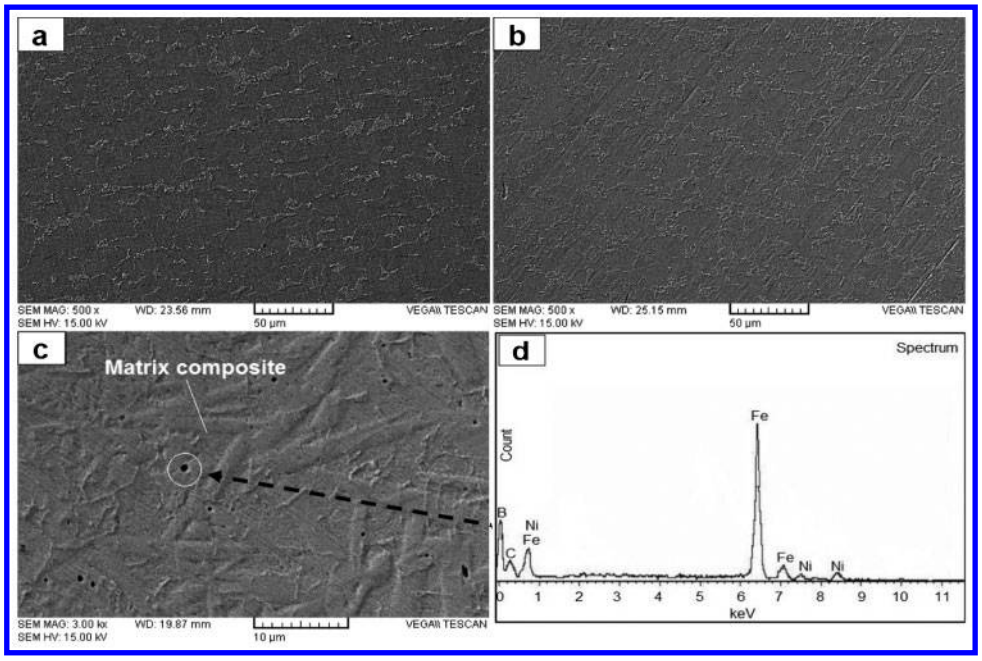

2 Images (SEM) of *a* base, *b* HAZ and *c* weld samples after being polished and etched in etchant solution and *d* EDX analysis of dark points in *c*

polishing pad and then were washed by distilled water and alcohol and dried in air. The connection of samples to copper wire using the multimeter was ensured. Classic corrosion cell including a reference electrode, a graphite counter electrode and a working electrode (the sample) was prepared. Open circuit potential E_{OCP} determination time was considered 7200 s for each.

Balance time for starting linear polarisation resistance (LPR) test was considered 10 s after determining E_{OCP}. Scanning speed was 0·5 mV s^{-1}. The potential application range was $\pm$20 mV relative to E_{OCP}.

Balance time for starting electrochemical impedance spectroscopy (EIS) test was considered 10 s after testing LPR. Electrochemical impedance spectroscopy curves with the applied sinus disturbance potential of 10 mV were obtained in the range of E_{OCP}. Frequency range was from 0·01 to 10^5 Hz. Starting potential E_{Start} equalled 0 V, and balance time for the next test was considered 10 s. The number of frequency was 78, and 11 data were read by the device in each frequency. Electrochemical Impendence Spectrum Analyser software was used for fitting and extracting the data of electrochemical impendence.

After 7 days and in the last test, potentiodynamic polarisation test was performed for all the three samples with 10 s of balance time. Scanning speed and E_{Step} were 0·0001 V s^{-1} and 1 mV respectively. Potential application range was $\pm$150 mV relative to E_{OCP}.

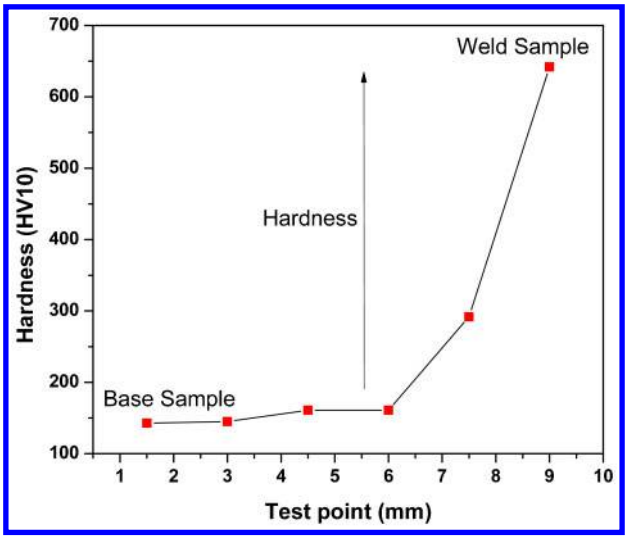

3 Hardness profile from base sample to end of weld sample in terms of Vickers (HV10)

Results and discussion

Microstructural characterisation

Images (SEM) of base, weld and HAZ samples after being polished and etched in the etchant solution and before corrosion tests are given in Fig. 2. As can be observed, structure of the HAZ sample in Fig. 2*b* was more coarse grained than that in base sample in Fig. 2*a*. Weight per cent of the elements existing in steel base sample was obtained by quantometer test, as mentioned in Table 1.

More measures are required for studying the chemical composition and structure of welding sample. First, an SEM image was taken from the composite sample; then, dark points were analysed in the structure. The point analysed in terms of EDX is specified in Fig. 2*c*, with the magnification of $\times$3000, and results of EDX analysis relating to this point are given in Fig. 2*d*. Accordingly, particles of boron, carbon, nickel and iron formed the composite's chemical composition at this point. Therefore, considering the more amount of boron than carbon in the EDX diagram, it is predicted that B_4C particles were available in this zone. Generally, it is predictable that B_4C particles along with nickel with irregular geometrical shape were dispersed non-uniformly in steel matrix.

Hardness gauging test

Hardness profile from base sample to end of weld sample in terms of HV10 is given in Fig. 3. As is seen,

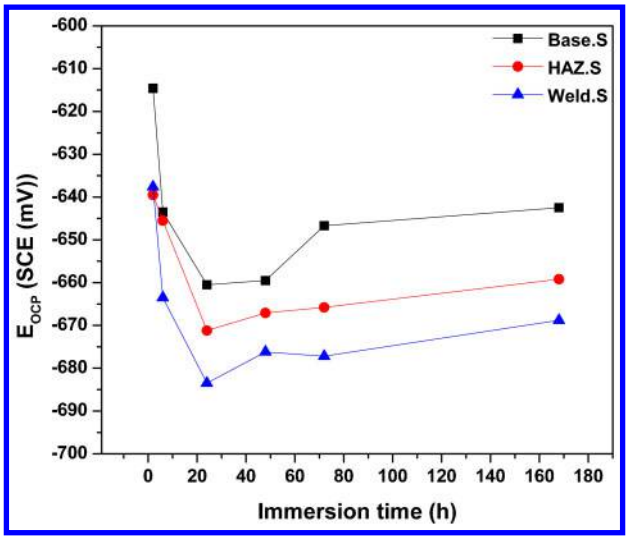

4 E_{OCP} data for all three samples immersed in 3·5 wt-%NaCl solution

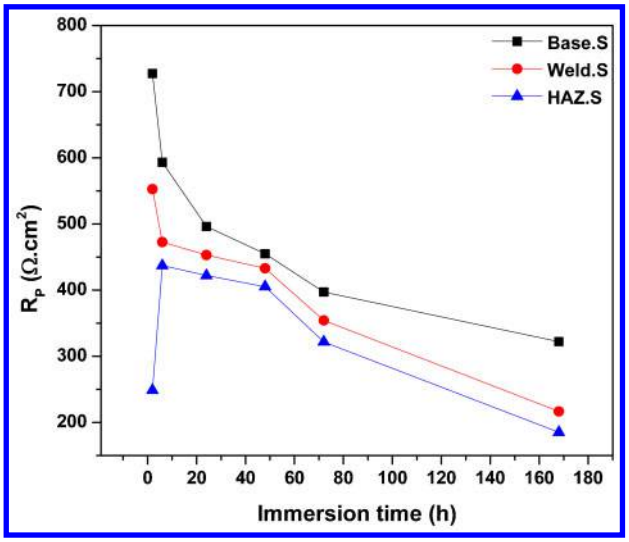

5 Linear polarisation resistance results for all three samples immersed in 3·5 wt-%NaCl solution

hardness of B_4C composite sample with plain carbon steel increased from base sample to the end of the manufactured weld sample from 145 to 642 HV10. This was due to the presence of boron carbide's strengthening particles in the composite structure. Therefore, hardness and consequently resistance to abrasion of plain carbon steel were locally increased by manufacturing this composite thereon.

Results of electrochemical tests

Open circuit potential variation with time

E_{OCP} values all three samples relative to different times of immersion in 3·5 wt-%NaCl solution is given in Fig. 4. As is observed, generally, E_{OCP} values of all three samples considerably decreased to about 30–50 mV in the early hours. After 25–30 h, it became constant and gradually increased over time up to 70 h. It is necessary to note that, at all times, the highest and lowest values of E_{OCP} were related to base sample and weld sample respectively. The value of E_{OCP} indicated nobility of metal surface; therefore, local manufacturing of composite and use of GTAW slightly decreased nobility of base metal in the composite zone. In order to appropriately judge and analyse the results of E_{OCP} in three samples at different immersion times, results of other electrochemical tests were also considered. Therefore, considering different electrochemical tests, corrosion trend of the samples was analysed in the corrosive solution.

Linear polarisation resistance test variation with time

The LPR values of all three samples after immersion in 3·5 wt-%NaCl solution at different times are given in Fig. 5. Therefore, by comparing values of R_P and their interpretation, a suitable conclusion can be obtained for analysing LPR data. As observed in Fig. 5, it seems that value of R_P for all three samples had a decreasing trend after immersion in the time interval of 2 h to 7 days. At all times, the base sample, HAZ sample and weld sample had the highest, lowest and average values R_P. In the time interval of 2 to 6 h after immersion, R_P of the HAZ sample had an increasing, decreasing and finally constant trend respectively. Moreover, in the time interval of 48 h to 7 days of immersion, it considerably deceased and reached R_P of the weld sample. It is predictable that the reason can be the formation of a surface layer in the time interval of 2–6 h of immersion and gradual dissolution of this layer over the immersion time. Considering the comparison of R_P values obtained from LPR and E_{OCP} relative to immersion time, it can be concluded that, although E_{OCP} value of weld sample was more negative than that of HAZ sample at all times of immersion, its R_P value was slightly more than that of HAZ sample at all times of immersion.

Electrochemical impedance spectroscopy test variation with time

The EIS diagram of all three samples at different times of immersion in 3·5 wt-%NaCl solution is given in Fig. 6. All EIS diagrams relating to all three samples at all times of immersion were analysed by an equivalent circuit, as depicted in Fig. 6*a*, inserted image. It is necessary to note that, in the base sample at all times of immersion and in the weld sample in the time interval of 2–6 h of immersion in corrosive solutions, Warburg diffusional element was not included in the equivalent circuit (Fig. 6*a*) due to the absence of diffusional behaviour of the samples. In order to precisely present the results obtained from fitting EIS data with the mentioned equivalent circuit, constant phase element (CPE) was used instead of capacity C. Admittance and impedance of CPE were defined as follows.[9]

Constant phase element admittance

$$Y_Q = P_0(J\omega)^n \quad (1)$$

Constant phase element impedance

$$Z_Q = \frac{1}{P_0}(J\omega)^{-n} \quad (2)$$

In these equations, Q is the CPE, P_0 (y_0) is the CPE module and n is the CPE phase. Because measured EIS rings were not full semicircular in the laboratory, CPE was used instead of C to analyse spectrums of EIS using the designed equivalent circuit. The exit degree of the EIS rings from the ideal state measured in the laboratory depends on phase n. In any case, CPE is a parallel composition of a pure capacitor and a resistance, the

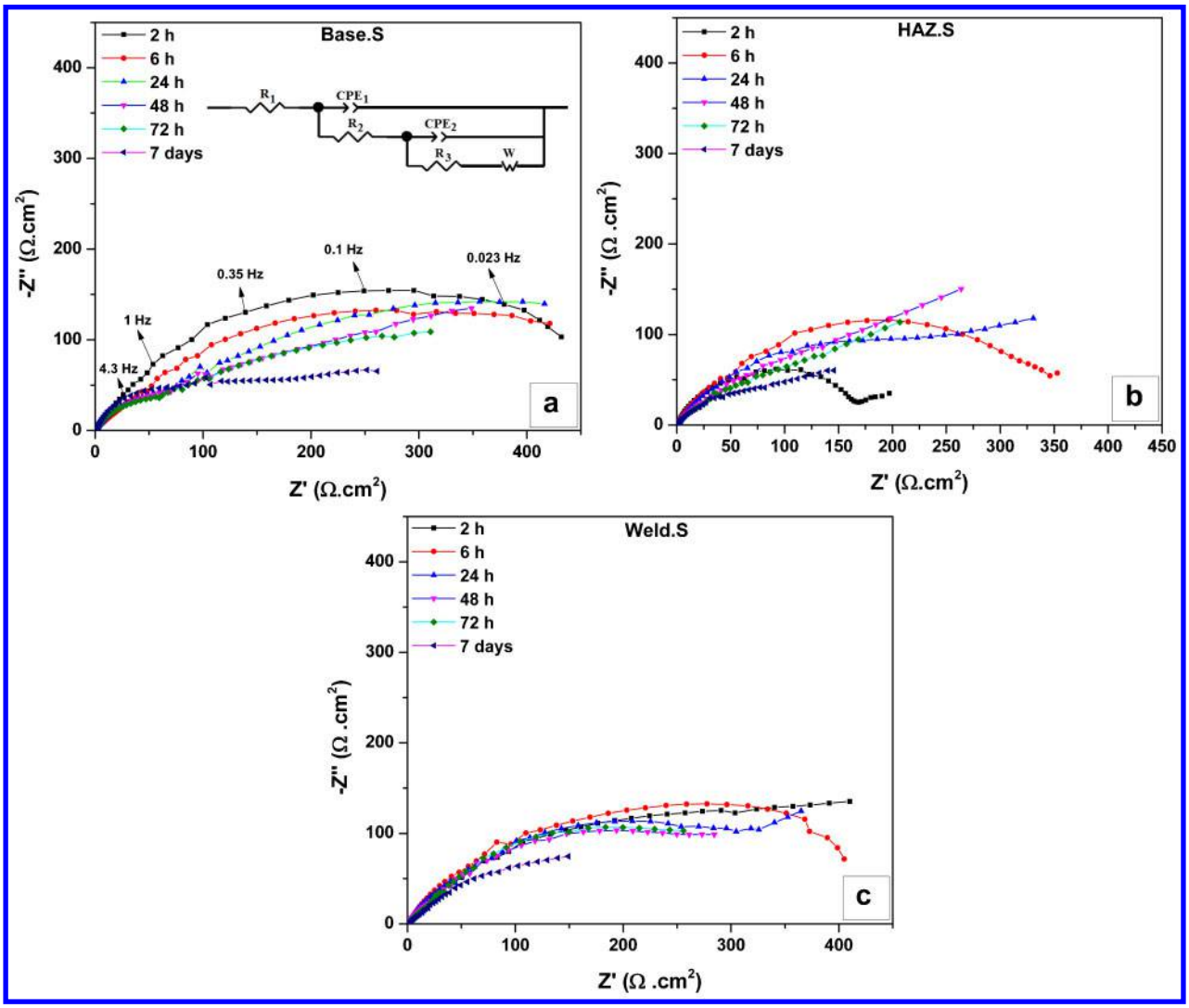

6 Nyqusit curves of all three samples at different times immersed in 3·5 wt-%NaCl solution; equivalent circuit used for EIS data fitting was inserted

impedance value of which is reversely in correspondence with angular frequency.[14] Relaxation time of τ for a parallel equivalent circuit composed of a CPE and a resistance can be defined as in equation (3)[15,16]

$$\tau_i = C_i R_i \tag{3}$$

In this equation, C_i is capacity of pure capacitor which forms CPE, and R_i is the resistance which constitutes CPE. The following relation holds among p_i (y_{oi}), n_i, τ_i and R_i

$$p_i = \frac{\tau_i^{n_i}}{R_i} \tag{4}$$

The following equation was obtained by combining equations (3) and (4)

$$C_i = \left[P_i R_i^{(1-n_i)}\right]^{\frac{1}{n_i}} \tag{5}$$

Based on equation (5), each of charge transfer capacity C_1 and surface layer capacity C_2 had their own CPE, as demonstrated in the equivalent circuit (Fig. 6*a*) of CPE_1 and CPE_2.

Because all EIS rings measured in the laboratory are related to crystalline solid in electrochemical interface, they seldom generate a full semicircle. Exit from the ideal state of EIS rings measured in the laboratory depends on roughness of solid electrode surface, heterogeneous physical and chemical nature of electrode, uniform and non-uniform current density distribution in electrode surface and coupling effect.[14] The required values of equivalent circuit elements for fitting EIS data of all three samples after immersion at different times are given in Table 2. The data relating to C_1 and C_2, which were calculated by equation (5), are presented in Table 2. To have logical and proper analysis for the EIS data obtained from the equivalent circuit relating to all three samples, changes of $C-t$, $n-t$ and $R-t$ are separately analysed for the first ring (surface layer) and the second ring (charge transfer layer) of the equivalent circuit. Therefore, the following can be given for each sample.

Base sample

Considering changes of C_1-t, n_1-t and R_2-t altogether in Table 2, which are related to surface layer of the base sample, it can be found that immersion of base sample in corrosive solution for 2–24 h increased capacity of its

Table 2 Extracted values of equivalent circuit elements from fitted EIS data of all three samples after immersion at different times

Immersion time	R_1/Ω cm^2	R_2/Ω cm^2	R_3/Ω cm^2	n_1	p_1	n_2	p_2	W/Ω cm^2	C_1/μF cm^{-2}	C_1/μF cm^{-2}
					Base sample					
2 h	0·8	37·1	458·3	0·71	$1{\cdot}86\times10^{-6}$	0·61	$6{\cdot}53\times10^{-6}$	···	0·95	0·15
6 h	0·8	39·7	527·5	0·72	$1{\cdot}18\times10^{-5}$	0·53	$2{\cdot}61\times10^{-5}$	···	0·59	0·58
24 h	0·9	58·3	703·6	0·77	$6{\cdot}08\times10^{-6}$	0·47	$4{\cdot}68\times10^{-5}$	···	0·56	0·99
48 h	1·0	61·4	714·5	0·80	$5{\cdot}90\times10^{-6}$	0·46	$5{\cdot}25\times10^{-5}$	···	0·81	1·11
72 h	1·1	67·5	458·6	0·77	$8{\cdot}14\times10^{-6}$	0·45	$7{\cdot}85\times10^{-5}$	···	0·86	1·35
7 days	1·3	104·9	302·3	0·80	$7{\cdot}46\times10^{-6}$	0·46	$10{\cdot}67\times10^{-5}$	···	1·55	1·89
					HAZ sample					
2 h	0·8	0·1	175·8	0·62	$9{\cdot}45\times10^{-6}$	0·89	$4{\cdot}38\times10^{-6}$	8·33	0·002	1·80
6 h	1·0	114. 6	334·6	0·69	$1{\cdot}81\times10^{-5}$	0·70	$1{\cdot}88\times10^{-5}$	9·50	1·12	2·14
24 h	1·0	61·8	232·0	0·68	$2{\cdot}54\times10^{-5}$	0·69	$2{\cdot}70\times10^{-5}$	23·90	1·21	2·76
48 h	1·1	55·7	179·9	0·65	$3{\cdot}83\times10^{-5}$	0·64	$5{\cdot}44\times10^{-5}$	14·61	1·39	4·03
72 h	1·2	43·2	130·4	0·66	$4{\cdot}87\times10^{-5}$	0·63	$7{\cdot}14\times10^{-5}$	12·36	2·03	4·58
7 days	1·4	26·0	114·0	0·65	$6{\cdot}86\times10^{-5}$	0·60	$10{\cdot}65\times10^{-5}$	10·01	2·27	5·62
					Weld sample					
2 h	0·8	7·60	427·4	0·88	$4{\cdot}17\times10^{-6}$	0·64	$2{\cdot}58\times10^{-5}$	···	1·01	2·04
6 h	0·8	126. 4	369·4	0·74	$1{\cdot}55\times10^{-5}$	0·65	$2{\cdot}76\times10^{-5}$	···	1·73	2·33
24 h	0·9	8·5	322·2	0·72	$2{\cdot}71\times10^{-5}$	0·68	$3{\cdot}21\times10^{-5}$	24·18	2·70	3·73
48 h	0·9	1·8	251·1	0·71	$3{\cdot}52\times10^{-5}$	0·66	$4{\cdot}12\times10^{-5}$	15·85	3·22	3·91
72 h	0·9	3·3	241·8	0·70	$5{\cdot}20\times10^{-5}$	0·65	$5{\cdot}46\times10^{-5}$	13·44	4·48	5·31
7 days	1·0	29·0	169·3	0·70	$6{\cdot}85\times10^{-5}$	0·64	$1{\cdot}16\times10^{-4}$	11·40	4·76	12·71

surface layer C_1 considering changes of C_1-t. Therefore, thickness of surface layer, which is reversely related to its capacity (according to equation (6)), would increase by 40%. In time interval of 24 h to 7 days of immersion, growth of surface layer of the base sample also decreased by 60% relative to the first 24 h. Moreover, considering R_2-t changes, 60% increase in polarisation resistance R_2 was observed, which was related to surface layer of the base sample in time interval of 2 h to 7 days of immersion in corrosive solution. In spite of the increase in capacity of the surface layer from 24 h to 7 days of immersion in corrosive solution, resistance of the surface layer also increased. Considering changes of n_1-t, it can be observed that the reason was 50% decrease in roughness of surface layer and increase in n_1 value during the increase in immersion time. Relation[1] holds between capacity and thickness of the surface layer or charge transfer

$$C=\frac{\varepsilon\varepsilon_0 A}{D} \tag{6}$$

In this relation, C is capacity of surface layer or charge transfer, A is active surface of electrode, ε is dielectric permeability coefficient of charge transfer layer in surface, ε_0 is dielectric permeability coefficient in vacuum and D is thickness of surface layer or charge transfer. Considering changes of C_2-t, n_2-t and R_3-t altogether in Table 2, which are related to charge transfer layer of the base sample, it can be found that immersion of base sample in corrosive solution for 2–24 h increased capacity of its surface layer C_2 considering changes of C_2-t. Therefore, thickness of charge transfer, which is reversely related to its capacity, would decrease by 90%. In addition, considering changes of n_2-t, 25% decrease in n_2 was observed concurrent with the decrease in thickness of the charge transfer capacity of base sample in the time interval of 2 h to 7 days of immersion in corrosive solution, which meant that roughness and porosity of charge transfer increased with the same value; as a result, base sample became rougher by 25% with the increase in immersion time. This roughness was originated from dissolution of base sample and exit of metal ions produced by the dissolution. It is necessary to note that these ions help produce the surface layer. Considering changes of R_3-t, polarisation resistance of R_3 relating to charge transfer layer of the base sample increased by 5% in time interval of 2 to 24 h was constant between 24 and 48 h and decreased by 50% between 48 h and 7 days. Increase in R_3 in time interval of 2–24 h of immersion in corrosive solution was because of the formation of surface layer on the charge transfer layer, which acted as a physical barrier for ion exchange. Therefore, despite the increase in charge transfer capacity in time interval of 2–24 h of immersion, R_3 resistance increased due to the presence of surface layer. With the increase in immersion time in time interval of 24 h to 7 days, R_3 resistance decreased with the dissolution of surface layer.

Heat affected zone sample

Considering changes of C_1-t, n_1-t and R_2-t altogether in Table 2, which are related to surface layer of HAZ sample, it can be found that, based on the changes of C_1-t, capacity of surface layer of C_1 increased considerably after immediate formation of this layer in the early hours of immersion of the HAZ sample in corrosive solution, which meant considerable decrease (90%) in thickness of surface layer of HAZ sample in time interval of 2 h to 7 days of immersion in the corrosive solution. Considering changes of n_1-t, it can be observed that roughness of surface layer was minimised (30%) within 2 to 6 h, which was concurrent with the formation of surface layer; when immersion time increased in time interval of 6 h to 7 days, roughness of the surface layer increased by 5% relative to the first 6 h of immersion in corrosive solution due to dissolution of surface layer. In addition, considering changes of R_2-t, it was found that resistance of surface layer R_2 in the early hours of immersion of the HAZ sample in corrosive solution increased from 0·1 to

114·6 Ω cm^2 due to immediate formation of surface layer. Therefore, despite increase in capacity of the surface layer in time interval of 2–6 h of immersion, R_2 resistance increased due to immediate formation of the surface layer and decrease in its roughness. With the increase in immersion time to the interval of 6 h to 7 days, R_2 resistance decreased by 70% relative to the first 6 h of immersion as a result of the dissolution of the surface layer. Considering changes of C_2-t, n_2-t and R_3-t altogether in Table 2, which are related to charge transfer layer of the HAZ sample, it can be found that, based on changes of C_2-t, charge transfer capacity increased considerably after immersion of HAZ sample in corrosive solution in time interval of 2 h to 7 days, which meant that thickness of charge transfer capacity decreased by 90%. Furthermore, considering changes of n_2-t, it can be found that decrease in thickness of charge transfer of the HAZ sample in time interval of 2 h to 7 days of immersion was concurrent with the roughness increase in charge transfer (30%). Moreover, considering changes of R_3-t, it can be observed that resistance of charge transfer R_3 increased by 40% and decreased by 60% in time intervals of 2–6 h and 6 h to 7 days respectively. The reasons can be attributed to the immediate formation of the surface layer in the early hours of immersion, increase in the related R_3 resistance and dissolution of the surface layer after 6 h to 7 days of immersion of HAZ sample. Therefore, despite the increase in charge transfer capacity of C_2 in time interval of 2–6 h of immersion of HAZ sample, R_3 resistance also increased.

Weld sample

Considering changes of C_1-t, n_1-t and R_2-t altogether in Table 2, which are related to surface layer of weld sample, it can be found that, according to changes of C_1-t, capacity of surface layer of C_1 increased considerably after immediate formation of this layer in the early hours of immersion of the weld sample in corrosive solution. This meant considerable thickness decrease (90%) of surface layer of weld sample in time interval of 2 h to 7 days of immersion in corrosive solution. Considering changes of n_1-t, it can be understood that decrease in thickness of surface layer of weld sample in time interval of 2 h to 7 days of immersion was concurrent with increase in roughness and porosity by 20%. Moreover, considering changes of R_2-t, it can be indicated that resistance of surface layer R_2 in the early hours of immersion of the weld sample in corrosive solution increased from 7·6 to 126·4 Ω cm^2 due to the immediate formation of surface layer despite the increase in capacity (30%) and roughness (15%). Then, with the increase in immersion time in time interval of 6 h to 7 days by dissolution and decrease in the thickness of surface layer, resistance also decreased relative to the first 6 h of immersion (70%). Considering changes of C_2-t, n_2-t and R_3-t altogether in Table 2 related to charge transfer layer of the weld sample, it can be found that C_2-t changes indicated considerable increase in charge transfer capacity C_2 after immersion of the weld sample in corrosive solution in time interval of 2 h to 7 days, i.e. thickness of charge transfer capacity decreased by 80%. Considering changes of R_3-t, it can be seen that thickness decrease in the charge transfer in weld sample in time interval of 2 h to 7 days of immersion was concurrent with the resistance decrease in charge transfer (60%). Although according to n_2-t changes, values of n_2 slightly fluctuated with the increase in immersion time, it is necessary to note that immediate formation of the surface layer after 6 h of immersion did not cause local increase in charge transfer resistance of R_3 unlike increase in charge transfer capacity. This may result from increase in porosity of surface layer despite the increase in R_3 after its immediate formation. The necessary condition for the presence of Warburg diffusional impedance was the presence of charge transfer layer with the minimum roughness. It is worth noting that the surface layer with low porosity can increase Warburg diffusional impedance. Therefore, it is predicted that, when roughness of both surface layer and charge transfer are low, Warburg diffusional impedance will emerge with high values. With the increase in immersion time and roughness of charge transfer, Warburg diffusional impedance also decreases. Considering values of polarisation resistance obtained from LPR test and resistance of charge transfer obtained from EIS, all three samples were observed at different immersion times. The results of both tests confirmed each other, and increasing and decreasing trends of polarisation resistance and, consequently, an equal corrosion behaviour were obtained in both cases.

Comparing EIS curves

For the purpose of appropriate and logical analysis and comparison of corrosive behaviour of all three samples, their related EIS curves (Nyqusit and Bode phase plots) after 2 h of immersion in 3·5 wt-%NaCl solutions are given in Fig. 7. It is necessary to note that EIS diagram of the samples with the equivalent circuit (Fig. 6*a*) was analysed under the mentioned condition. The required values of equivalent circuit elements for fitting EIS data of all the three samples are given in Table 3. For appropriate and logical analysis of the EIS data obtained with the equivalent circuit related to all three samples in (Table 3), first, n_1, C_1 and R_2 are studied for the first ring (surface layer) and then n_2, C_2 and R_3 are studied for the second ring (charge transfer layer) of the equivalent circuit related to all three samples. Considering values of n_1, C_1 and R_2 in Table 3, it is observed in all three samples that surface layer of base sample had average thickness (average capacity C_1 of 0·95 μF cm^{-2}), average porosity and roughness (29%) (average n_1) and very high R_2 resistance (37·1 Ω cm^2) in the corrosive solution after 2 h of immersion compared with other samples. Surface layer of the HAZ sample had the highest thickness (the lowest capacity C_1 of 0·002 μF cm^{-2}), highest porosity and roughness (38%) and lowest resistance (0·1 Ω cm^2) compared with other samples, and surface layer of the weld sample had the lowest thickness (highest capacity C_1 of 1·01 μF cm^{-2}) and lowest porosity and roughness (7·66%) due to low roughness (12%). Surface layer of the base sample had the highest R_2 resistance compared with the surface layer of other samples due to having high thickness and low porosity at the same time. Although the surface layer of HAZ sample had the highest thickness, it had the lowest resistance compared with the surface layer of other samples because of its high roughness. Similarly, although the surface layer of weld sample had the lowest roughness (12%), it had average resistance compared with the surface layer of other samples due to its low thickness. Considering values of

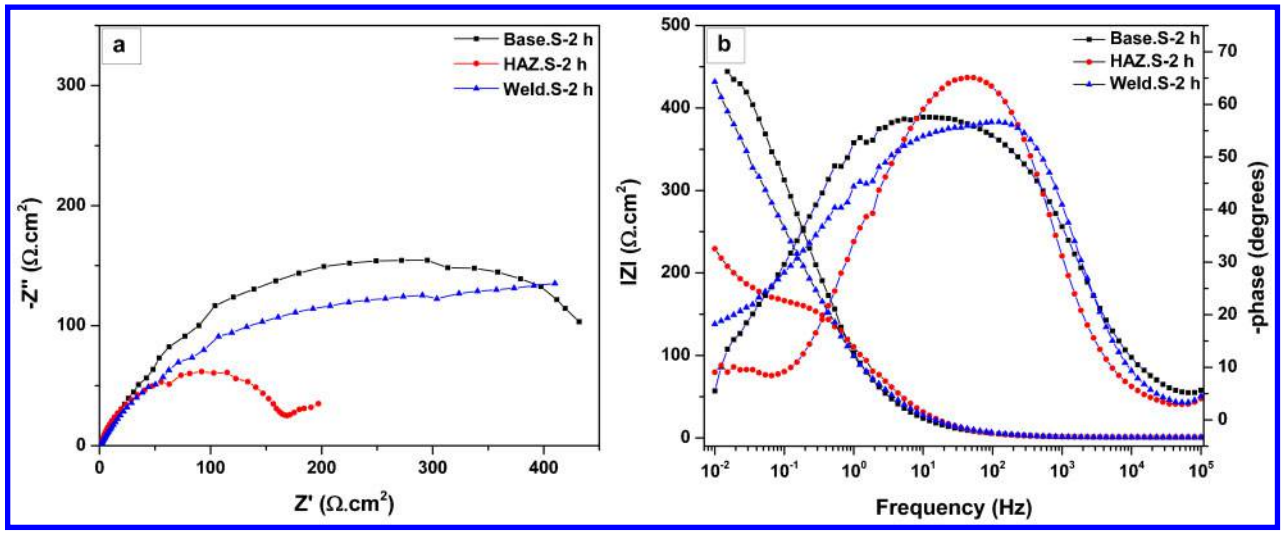

7 ***a*** **Nyquist and** ***b*** **Bode phase plots of all three samples after 2 h immersion in 3·5 wt-%NaCl solution**

n_2, C_2 and R_3 in Table 3, it can be found that the base sample had the charge transfer layer with the highest thickness (10–15 times), lowest capacity (C_2), highest roughness (40%) and highest R_3 resistance (458·3 Ω cm^2) compared with charge transfer layer of other samples. The presence of surface layer with high thickness and R_2 resistance in the base sample led to the protection of charge transfer layer with very high roughness compared with other samples against the corrosive environment, which itself caused increase in its R_3 resistance compared with charge transfer layer of other samples in spite of higher roughness. It is necessary to note that the presence of high roughness of charge transfer layer in the base sample caused no Warburg diffusional impedance in corrosion mechanism of the base sample. In addition, the charge transfer layer of the weld sample had almost the same thickness (relatively the same capacity C_2 of 2·04 μF cm^{-2}), higher R_2 resistance (427·4 Ω cm^2) and higher roughness (25%) compared with charge transfer layer of HAZ sample. The presence of thin surface layer with very low roughness and higher R_2 resistance than surface layer of HAZ sample caused increase in R_3 resistance of charge transfer layer of the weld sample compared with the HAZ sample (55%), although it did not reach the R_3 of charge transfer layer of the base sample. Therefore, corrosion status of the base sample was more desirable than that of other samples after 2 h of immersion in the corrosive solution. It is necessary to note that the presence of low roughness in the charge transfer layer of HAZ sample caused Warburg diffusional impedance in its relevant EIS curve after 2 h of immersion in the corrosive solution. In general, this trend was maintained at all times of immersion; the only explanation can be that resistance of the surface layer of base sample slightly increased and its roughness decreased in time interval of 2 h to 7 days compared with other samples. Moreover, HAZ and weld samples had a diffusional behaviour due to low porosity of charge transfer layer compared with the base sample. After 2 h to 7 days of immersion, Warburg diffusional impedance relating to these samples decreased. Generally, the weld sample had higher Warburg diffusional impedance because of lower porosity both in the surface and in charge transfer layer.

Potentiodynamic polarisation test

Since all previous electrochemical tests performed on samples during 7 days were non-destructive techniques, potentiodynamic polarisation diagram of the corrosion samples after 7 days of immersion in 3·5 wt-%NaCl solution is given in Fig. 8, and the data relating to this diagram are presented in Table 4. As can be observed,

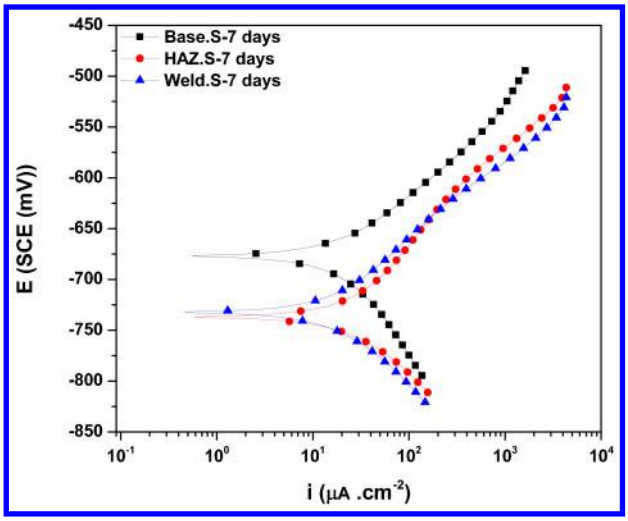

8 Potentiodynamic polarisation diagram of corrosion samples after 7 days of immersion in 3·5 wt-%NaCl solution

Table 3 Extracted values of equivalent circuit elements for fitted EIS data of all three samples after 2 h of immersion in 3·5 wt-%NaCl solution

Sample	R_1/Ω cm^2	R_2/Ω cm^2	R_3/Ω cm^2	n_1	p_1	n_2	p_2	W/Ω cm^2	C_1/μF cm^{-2}	C_1/μF cm^{-2}
Base	0·8	37·1	458·3	0·71	$1{\cdot}86\times10^{-5}$	0·61	$6{\cdot}53\times10^{-6}$	···	0·95	0·15
Weld	0·8	7·60	427·4	0·88	$4{\cdot}17\times10^{-6}$	0·64	$2{\cdot}58\times10^{-5}$	···	1·01	2·04
HAZ	0·8	0·1	175·8	0·62	$9{\cdot}45\times10^{-6}$	0·89	$4{\cdot}38\times10^{-6}$	8·33	0·002	1·80

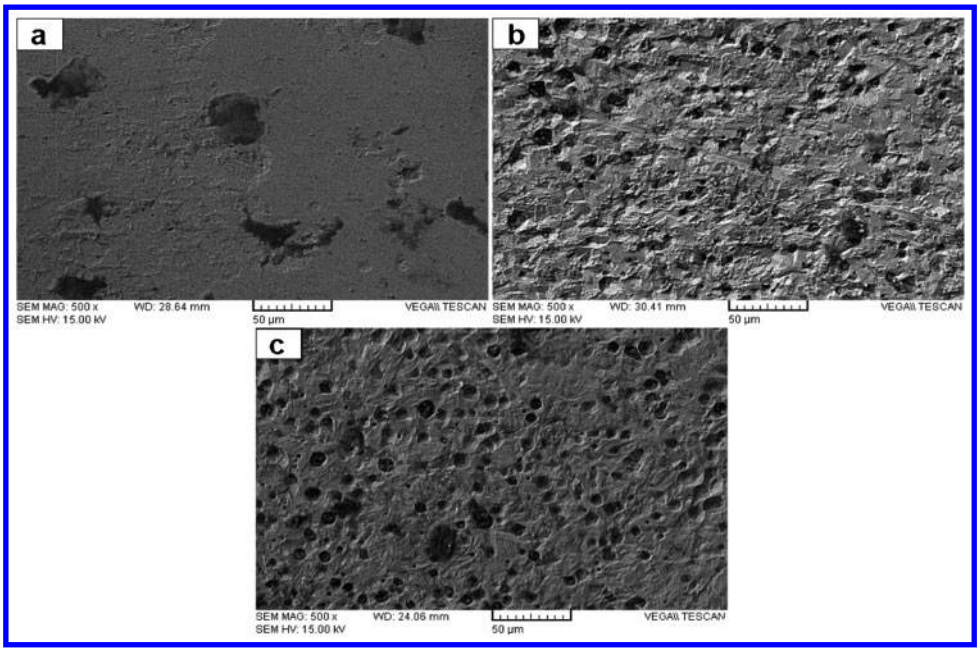

9 Images (SEM) of corrosion attacks on *a* base, *b* HAZ and *c* weld samples after 4 days immersion in 3·5 wt-%NaCl solution

while corrosion potential of the HAZ sample was more negative than that of the weld sample and base sample in the same order, corrosion current i_{Corr} of this sample was higher than that of the weld and base samples. It is necessary to note that, in potentiodynamic polarisation test of three samples after immersion in corrosive environment, corrosion current of the weld sample decreased compared with that of HAZ sample after 7 days of immersion in corrosive solution despite more negative E_{OCP} value of the weld sample compared with the HAZ sample. Therefore, after 7 days of immersion in corrosive environment, corrosion rate of the base sample was lower than that of the weld and HAZ samples in this order. Consequently, results of LPR and potentiodynamic polarisation tests confirmed each other.

Microstructural studies after corrosion tests

Image (SEM) of corrosion attacks of the base, HAZ and weld samples was prepared after 4 days immersion is given in Fig. 9. As can be observed, corrosion structure of the base sample had fewer corrosion products than other samples, and its surface was less affected by corrosive ions in 3·5 wt-%NaCl solution. In contrast, considering corrosion structure images of the weld and HAZ samples, it can be observed that surface of HAZ sample was intensively affected by corrosive ions compared with other samples in 3·5 wt-%NaCl solutions, and the weld sample was on the borderline. Therefore, SEM images showed higher resistance to corrosion in the base sample compared with the weld and HAZ samples.

Electrochemical reactions conducted during corrosion

The following electrochemical reactions occurred in corrosion process of all three samples. It is necessary to note that because carbide particles such as B_4C had more positive electrochemical potential in the weld sample than the steel matrix, it is predicted that galvanic corrosion will locally occur around B_4C particles in the composite surface.[17] Therefore, the surroundings of B_4C particles are suitable places for performing anodic reactions. The schematics of electrochemical processes during corrosion of weld sample in 3·5 wt-%NaCl solution is given in Fig. 10. Anodic reacion

$$Fe_{(s)} \rightarrow Fe^{2+}_{(aq)} + 2e^- \quad (7)$$

Cathodic reaction

$$O_{2\,(g)} + 2\,H_2O_{(l)} + 4e^- \rightarrow 4OH^-_{(aq)} \quad (8)$$

General reaction

$$2Fe_{(s)} + O_{2\,(g)} + 2H_2O_{(l)} \rightarrow 2\,Fe^{2+}_{(aq)} + 4OH^-_{(aq)} \quad (9)$$

Then, the following can be given

$$Fe^{2+}_{(aq)} + 2OH^-_{(aq)} \rightarrow Fe(OH)_{2(s)} \quad (10)$$

Table 4 Potentiodynamic polarisation extracted data of all three samples after 7 days of immersion in 3·5 wt-%NaCl solution

Sample	E_{corr}/mV(SCE*)	β_a/V/decade	β_c/V/decade	i_{corr}/µA cm^{-2}	Corrosion rate/mm/year
Base	−679·2	0·063	−0·081	13·90	0·16
Weld	−724·1	0·077	−0·079	16·30	0·19
HAZ	−732·2	0·079	−0·074	19·20	0·22

*SCE: saturated calomel electrode.

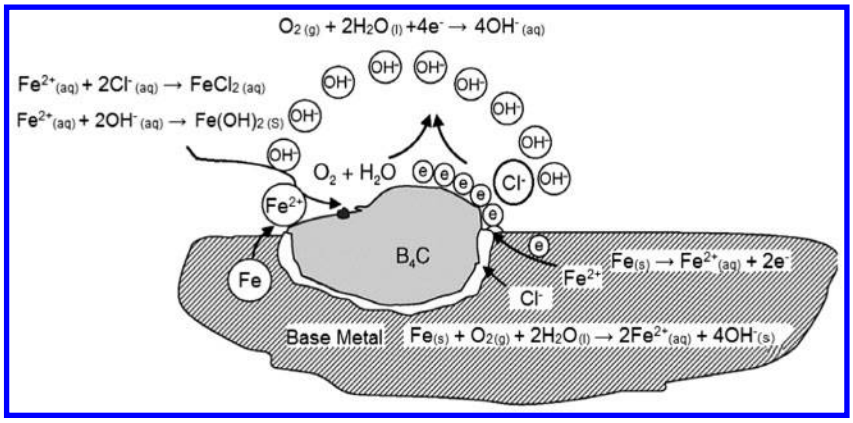

10 Schematics of electrochemical processes during corrosion of weld sample in 3·5 wt-%NaCl solution

Considering the presence of chloride ion in corrosive environment

$$Fe^{2+}_{(aq)} + 2Cl^-_{(aq)} \rightarrow FeCl_{2(aq)} \quad (11)$$

Most carbide particles such as B_4C do not react and are not ionised in water environments; therefore, they do not participate in electrochemical reactions in the environment containing chlorine ion and oxygen. Considering the point that these carbide particles such as B_4C have more positive electrochemical potential than steel matrix, they play the cathodic role in composite surface and their surroundings are suitable places for anodic reactions. Therefore, galvanic corrosion will be possible around carbide particles. In fact, in dark zones of the SEM image of B_4C composite structure, oxygen reduction will be reduced compared with the surrounding zones, and subsequently, galvanic corrosion resulting from increase in cathodic processes will be strengthened due to the presence of B_4C strengthening.[18] As shown in Fig. 10, precipitates like iron hydroxide [$Fe(OH)_2$] and iron chloride ($FeCl_2$) help create a surface layer in the surface of carbide particles and steel matrix because of the reduction of oxygen ions around and on the surface of carbide particles and considering the presence of chlorine ion in the corrosive solution.

Conclusions

1. The corrosion behaviour of MMC plain carbon steel–B_4C was studied in 3·5 wt-%NaCl solution. Microstructural studies before corrosion confirmed the presence of B_4C and nickel particles in the made composite's steel matrix.

2. Hardness value of B_4C–plain carbon steel composite showed that the manufactured composite locally increased hardness of plain carbon steel from 145 to 642 HV10.

3. Electrochemical techniques showed that polarisation resistance R_p or charge transfer resistance R_3 of HAZ sample was lower than those of weld and base samples.

4. The results of microstructural studies of samples after corrosion showed that structure of the HAZ sample was more affected by the corrosive ions compared with weld and base samples.

5. Main corrosion product of the samples was iron hydroxide [$Fe(OH)_2$], which helped to form a surface layer. It is necessary to note that the presence of chlorine ion in corrosive solution helped create surface layer by forming precipitates such as iron chloride ($FeCl_2$).

Acknowledgements

Authors would like to acknowledge the Khorasan Razavi, Science and Research Branch, Islamic Azad University, Neyshabur, Iran for providing experimental facilities.

References

1. V. A. Katkar, G. Gunasekaran, A. G. Rao and P. M. Koli: 'Effect of the reinforced boron carbide particulate content of AA6061 alloy on formation of the passive film in seawater', *Corros. Sci.*, 2011, **53**, 2700–2712.
2. M. Gladkovas, V. Medeliene, M. Samuleviciene and E. Juzeliunas: 'Corrosion study of electroplated nickel metal-matrix composites B_4C, Al_2O_3 and SiC', *Chemija*, 2002, **13**, 36–40.
3. D. D. Radev, Z. T. Zakhariev and M. A. Marinitch: 'Corrosion resistance of B_4C-Me_xB_y composite materials', *J. Alloys Compd*, 1993, **196**, 93–96.
4. M. T. Siniawski, S. J. Harris, Q. Wang and S. Liu: 'Wear initiation of 52100 steel sliding against a thin boron carbide coating', *Tribol. Lett.*, 2003, **15**, 29–41.
5. W. Mingchao, Z. Zuoguang, S. Zhijie and L. Min: 'Effect of fiber type on mechanical properties of short carbon fiber reinforced B_4C composites', *Ceram. Int.*, 2009, **35**, 1461–1466.
6. A. Alizadeh, E. Taheri-Nassaj and M. Hajizamani: 'Hot extrusion process effect on mechanical behavior of stir cast Al based composites reinforced with mechanically milled B4C nanoparticles', *J. Mater. Sci. Technol.*, 2011, **27**, 1113–1119.
7. V. Medeliene: 'The influence of B_4C and SiC additions on the morphological, physical, chemical and corrosion properties of Ni coatings', *Coat. Technol.*, 2002, **154**, 104–111.
8. T. Eckardta, K. Bewilogua, G. van der Kolk, T. Hurkmans, T. Trinh and W. Fleischer: 'Improving tribological properties of sputtered boron carbide coatings by process modifications', *Surf. Coat. Technol.*, 2000, **126**, 69–75.
9. W. Zhang, L. Gao, J. Lia, J. Yang and Y. Yin: 'TiAl/B_4C marine material-fabrication, mechanical and corrosion properties', *Ceram. Int.*, 2011, **37**, 783–789.
10. S. K. Singh and A. K. Mukherjee: 'Kinetics of mild steel corrosion in aqueous acetic acid solutions', *J. Mater. Sci. Technol.*, 2010, **26**, 264–269.
11. A. Araghi and M. H. Paydar: 'Electroless deposition of Ni–P–B_4C composite coating on AZ91D magnesium alloy and investigation on its wear and corrosion resistance', *Mater. Des.*, 2010, **31**, 3095–3099.
12. H. Ding, G. A. Hawthorn and L. H. Hihara: 'Inhibitive effect of seawater on the corrosion of particulate-reinforced aluminum-matrix composites and monolithic aluminum alloy', *J. Electrochem. Soc.*, 2009, **156**, C352–C359.
13. C. Guedes Soares, Y. Garbatov and A. Zayed: 'Effect of environment factors on steel plate corrosion under marine immersion conditions', *Corros. Eng. Sci. Technol.*, 2011, **46**, 524–541.

14. H. Ma, X. Cheng, G. Li, S. Chen, Z. Quan, S. Zhao and L. Niu: 'The influence of hydrogen sulfide on corrosion of iron under different conditions', *Corros. Sci.*, 2000, **42**, 1669–1683.
15. E. McCafferty: 'Introduction to corrosion science', 575; 2010, Washington, DC, Springer Science.
16. I. Danaee, M. Niknejad Khomami and A. A. Attar: 'Corrosion of AISI 4130 steel alloy under hydrodynamic condition in ethylene glycol + water + NO^{-}_{2} solution', *J. Mater. Sci. Technol.*, 2013, **29**, 89–96.
17. Y. Han, D. Gallant and X. G. Chen: 'Investigation on corrosion behavior of the Al-B_4C metal matrix composite in a mildly oxidizing aqueous environment', *Corrosion*, 2011, **67**, 1150051–11.
18. H. Ding and L. H. Hihara: 'Electrochemical examinations on the corrosion behavior of boron carbide reinforced aluminum-matrix composites', *J. Electrochem. Soc.*, 2011, **158**, C118–C124.